Excited-State Absorption and Ultrafast Relaxation Dynamics of Porphyrin, Diprotonated Porphyrin, and Tetraoxaporphyrin Dication

Agnese Marcelli

Laboratorio Europeo di Spettroscopie non Lineari (LENS), Universitá di Firenze, via N. Carrara 1, 50019 Sesto Fiorentino, Firenze, Italy

Paolo Foggi[†]

Dipartimento di Chimica, Universitá di Perugia, via Elce di Sotto 8, 06123 Perugia, Italy

Laura Moroni, Cristina Gellini, and Pier Remigio Salvi*

Dipartimento di Chimica, Universitá di Firenze, via della Lastruccia 3, 50019 Sesto Fiorentino, Firenze, Italy

Received: October 18, 2007; In Final Form: December 11, 2007

The relaxation dynamics of unsubstituted porphyrin (H_2P), diprotonated porphyrin (H_4P^{2+}), and tetraoxaporphyrin dication ($TOxP^{2+}$) has been investigated in the femtosecond−nanosecond time domain upon photoexcitation in the Soret band with pulses of femtosecond duration. By probing with spectrally broad femtosecond pulses, we have observed transient absorption spectra at delay times up to 1.5 ns. The kinetic profiles corresponding with the band maxima due to excited-state absorption have been determined for the three species. Four components of the relaxation process are distinguished for H_2P: the unresolvably short $B \rightarrow Q_y$ internal conversion is followed by the $Q_y \rightarrow Q_x$ process, vibrational relaxation, and thermalization in the Q_x state with time constant ≈150 fs, 1.8 ps, and 24.9 ps, respectively. Going from H_2P to $TOxP^{2+}$, two processes are resolved, i.e., $B \rightarrow Q$ internal conversion and thermal equilibration in the Q state. The $B \rightarrow Q$ time constant has been determined to be 25 ps. The large difference with respect to the $B \rightarrow Q_y$ time constant of H_2P has been related to the increased energy gap between the coupled states, 9370 cm^{-1} in $TOxP^{2+}$ vs 6100 cm^{-1} in H_2P. The relaxation dynamics of H_4P^{2+} has a first ultrafast component of ≈300 fs assigned as internal conversion between the B (or Soret) state and charge-transfer (CT) states of the H_4P^{2+} complex with two trifluoroacetate counterions. This process is followed by internal $CT \rightarrow Q$ conversion (time constant 9 ps) and thermalization in the Q state (time constant 22 ps).

I. Introduction

Porphyrins contribute to several biological and chemical processes of fundamental interest, which often involve their short-lived excited electronic states.[1] The most prominent example is chlorophyll behaving as a natural antenna for solar energy collection and as an electron donor, funneling the absorbed energy to the reaction center.[2] Supramolecular light-harvesting assemblies employing porphyrins[3] have been also synthesized for efficient electron transfer after photoexcitation.[4,5] In material science, the extremely large nonlinear optical susceptibilities of porphyrin linear arrays and oligomers, obtained by clever combination of porphyrin moieties,[6−8] are related, among other factors, to the high polarizability of these π-electron systems, i.e., to the whole set of their excited states. In the context of photodynamic therapy it is worth recalling that hematoporphyrin in the lowest triplet state acts as a photosensitizer for the generation of excited singlet oxygen.[9]

To acquire a deeper knowledge of the fast/ultrafast processes occurring in biological photoreceptors as well as in synthetic analogues, the relaxation dynamics from the lowest $\pi\pi^*$ states of monomer porphyrins, both as free bases and as metal complexes, have been investigated in great detail.[10−20] In tetraphenylporphyrin (H_2TPP; D_{2h} ring symmetry) the internal conversions $B \rightarrow Q_y$ and $Q_y \rightarrow Q_x$ starting from vibrationally excited levels of the Soret (or B) band take place in less than 50 and 100 fs, respectively.[10] Three decay processes have been observed in the lowest excited state (traditionally denoted as Q_x): intramolecular vibrational redistribution by dephasing and by elastic collisions with solvent molecules, with time constants 100−200 fs and 1.4 ps, and thermal equilibration or cooling by energy transfer to the solvent in the temporal range 10−20 ps. Similar results were reported for a second porphyrin derivative,[21] the only difference being the assignment of the intermediate time constant, 1.5 ps, to vibrational relaxation in the Q_x state.[12] As to D_{4h} metalloporphyrins, the most extensively studied is zinc tetraphenylporphyrin (ZnTPP).[14,15,17−19] The B lifetime in benzene and ethanol solution was measured by fluorescence up-conversion techniques, resulting 1.45 and 2.35 ps, respectively.[14,15] Further, among gas-phase metalloporphyrins ZnTPP has the longest B lifetime, 600 fs, in contrast with the ultrafast lifetimes of porphyrin complexes with transition metals having partially filled d orbitals, which fall in the range 50−100 fs.[19] It was concluded that although Zn(II) influences only indirectly the decay, other transition metal ions partecipate

* Author to whom correspondence should be addressed. E-mail: piero.salvi@unifi.it.

† Also at Laboratorio Europeo di Spettroscopie non Lineari (LENS), Universitá di Firenze, via N. Carrara 1, 50019 Sesto Fiorentino Firenze, Italy, and at INOA-CNR, Largo E. Fermi 6, 50125 Firenze, Italy.

10.1021/jp710132s CCC: $40.75
Published on Web 02/08/2008

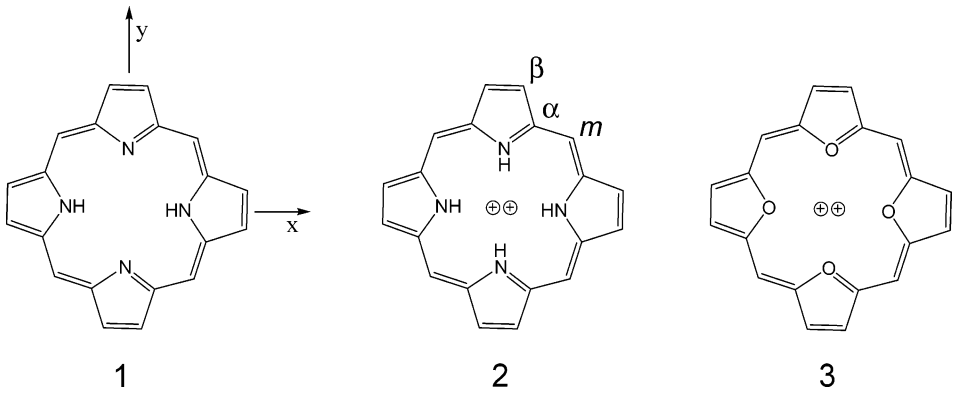

Figure 1. Molecular structures of porphyrin **1**, diprotonated porphyrin **2**, and tetraoxaporphyrin dication **3**. The reference system, common to the three species, is shown for convenience on **1**. The α, *β*, and *meso* positions are indicated on **2**.

actively in the process with the formation of a charge-transfer state from the porphyrin macrocycle to d orbitals. Thus, the presence of a central metal atom modulates considerably the photophysical properties of the porphyrin core.

Distortion from planarity in diprotonated porphyrin (H_4P^{2+}) and isoelectronic replacement of the inner nitrogen groups in tetraoxaporphyrin ($TOxP^{2+}$), the dicationic analogue of unsubstituted porphyrin (H_2P), are additional structural factors that may affect the relaxation dynamics of the photoexcited macrocycle. For the sake of clarity, the structures of H_2P, H_4P^{2+} and $TOxP^{2+}$, are drawn in Figure 1 as **1**, **2**, and **3**. In recent years we have reported on the vibrational and electronic properties of these systems.[22,23] In particular, a dual fluorescence, from both the first and the second excited state, was observed for $TOxP^{2+}$. The S_1 (or Q) quantum yield results to be 0.11 and the S_1 lifetime 7.2 ns. The S_2 (or B) state shows a surprisingly high quantum yield, 0.035, and a lifetime less than (or of the order of) the time resolution of our experimental apparatus, ≤100 ps. The near coincidence between absorption/fluorescence S_1 origins, the extremely small S_2 Stokes shift, and the clear mirror symmetry between the absorption and fluorescence spectra suggest that the D_{4h} ground state symmetry of $TOxP^{2+}$ is conserved in the S_1 and S_2 states and no significant reorganization of the solvent molecules around excited $TOxP^{2+}$ occurs. With reference to a previous definition,[24] **3** has been classified as a normal porphyrin analogue.[23] As to the diprotonated porphyrin **2**, there are experimental indications on peripherally substituted derivatives[25] and computational results on **2**[22,26,27] that the lowest energy macrocycle conformation in the ground state is nonplanar, i.e., saddle-shaped with D_{2d} symmetry, due to the steric interactions between the four central hydrogen atoms. Because of nonplanarity and consequent increase of the conformational freedom in the S_1 state,[24,28] the Q lifetime was found to be shorter than for **1**, 5.5 ns vs 15.8 ns.[23] However, it was not possible to measure the B lifetime exciting directly in the Soret band. In fact, this parameter was estimated to be in the femtosecond time scale from fluorescence yield and radiative lifetime,[23] well below our time resolution. All these considerations led us to investigate further on the relaxation dynamics of **2** and **3** in the femtosecond/picosecond time domain by means of transient absorption spectroscopy. In this paper we wish to give a full account of our results obtained exciting by femtosecond pulses the three molecular systems, **1**, **2** and **3**, in the Soret band and probing the time evolution with spectrally broad femtosecond pulses.

II. Materials and Methods

Free base porphyrin (or porphine, H_2P) **1** was purchased from Frontier Scientific (USA) and used without further purification. H_4P^{2+}, the diprotonated species **2**, was obtained by addition of a small amount (5% in volume) of trifluoroacetic acid to the benzene/cyclohexane (1:10) solution of **1**. The **1** → **2** conversion is quantitative.[29] The perchlorate salt of $TOxP^{2+}$ has been synthesized[30] and provided as a generous gift by Prof. E. Vogel (University of Köln, Germany).

Transient absorption experiments were carried out at room temperature with freshly prepared solutions of **1**−**3** using as solvents concentrated $HClO_4$ for **3** and the benzene/cyclohexane (1:10) mixture for **1** and **2**. The solvent combination was suggested by the necessity of reducing to a negligible level the undesired two-photon transient signal from benzene generated exciting into the Soret band of **1** and **2**, yet dissolving the solute completely. The solution concentration was adjusted such that the absorbance at the exciting wavelengths, 370 and 400 nm in a 2 mm thick cell, was ≈0.8. As to **1**, with a second excitation at 490 nm and the same cell thickness the absorbance A_{490} was set to 0.5. The sample was excited with pulse energy varying between 0.3 and 0.8 μJ. The transient signal was found to be proportional to the energy of the pump pulse. The solution stability under irradiation was checked by measuring the ground state absorption spectra before and after each experiment. No appreciable change was noticed, thus ruling out any photophysical degradation of our samples. For the sake of convenience the spectra of **1**−**3** solutions, $c \approx 10^{-5}$ M, are displayed in Figure 2.

Pump and probe experiments have been performed exciting **1** at 400 and 490 nm, **2** at 400 nm and **3** at 370 nm. The excitation wavelengths are indicated by arrows in Figure 2. The instrumental apparatus has been described in detail elsewhere.[31] A self-mode-locked Ti:sapphire laser (Spectra Physics, Tsunami) is pumped by an intracavity frequency doubled continuous wave (cw) Nd:YVO laser (Spectra Physics, Millennia) and emits pulses with ≈70 fs duration at 800 nm that are stretched, amplified, and recompressed by a regenerative amplifier (BMI Alpha 1000). The amplified pulses, whose temporal width is ≈100 fs, deliver an average power of ≈600 mW at 1 kHz repetition rate. The pulse train is divided into two portions of unequal intensity. The most intense is the excitation beam, which can be tuned by means of optical generation and amplification in a BBO crystal.[32] By frequency doubling the fundamental 800 nm radiation, we obtain light pulses at 400 nm. The 370 nm wavelength is obtained as fourth harmonic of the 1480 nm infrared beam generated in the BBO crystal. In a series of

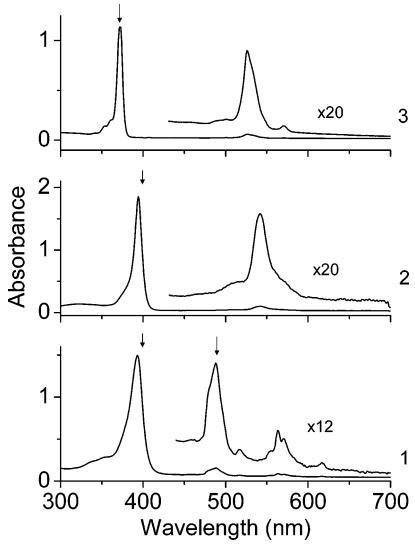

Figure 2. Absorption spectra of **1**−**3** solutions, $c \approx 10^{-5}$ M, room temperature, from bottom to top. The solvents are benzene/cyclohexane 1:10 for **1**, benzene/cyclohexane 1:10 added with CF_3COOH (5% in volume) for **2**, concentrated $HClO_4$ for **3**. Vertical arrows indicate pump wavelengths in our pump−probe experiments in the three cases.

experiments on **1** the 1265 nm radiation produced by the same crystal has been frequency-mixed with that at 800 nm to give light at 490 nm. The weakest portion of light, 1−2 mW, is focused on a CaF_2 plate and produces spectrally broad, i.e., containing all wavelengths between 350 and 650 nm ("white continuum"), femtosecond pulses. This beam is further split into two parts of equal intensity by a 50/50 beam splitter, the probe beam reaching the sample at a given time after the excitation pulse thanks to a suitable optical delay line and the reference beam travelling along a shorter path and then striking the sample before excitation. The three linearly polarized beams are focused on the solution by means of a parabolic mirror in a quasi-collinear geometry. The relative pump−probe polarization angle is set equal to 54.7° with the purpose of excluding from the excited-state dynamics rotational relaxation processes arising from the partial orientation of the molecules in the polarized light field. The solutions of **1**−**3** contained in the 2 mm thick quartz cell are kept under continuous stirring by means of a small magnet and irradiated at 100 Hz repetition rate by interposing a mechanical chopper along the primary excitation beam path to minimize spurious photochemical effects. Beyond the solution cell a single 25 cm Czerny-Turner monochromator (Chromex 250) and the coupled back-illuminated CCD camera (Princeton Instruments; response spectral range 300−1000 nm) are the dispersion and detection elements of the probe and reference beam. At any given delay time τ and wavelength λ the transient trasmittance $T(\tau,\lambda)$ is measured by $I(\tau,\lambda)/I_0(\lambda)$ where $I(\tau,\lambda)$ and $I_0(\lambda)$ are the intensities of the probe and reference beam.[31] The experiments described for **1**−**3** were repeated on blank solutions. No transient signal, except that due to the stimulated Raman gain from the solvent, was observed.

Due to the chirping of the spectrally broad probe pulse the red components of the white continuum speed over the blue components so that probing in the two visible regions does not occur at the same delay time.[33] In the first picosecond the effect causes experimental artifacts of considerable entity. To avoid such an inconvenience, we have determined the additional contribution to the delay time as a function of wavelength measuring the optical Kerr effect on the solution and using optically heterodyne detection, as it has been already reported.[31] Accordingly, the transient spectra measured in the first picoseconds have been corrected and reconstructed with the help of a homemade correction program taking into account the plot of time vs wavelength. The transient absorbance $\Delta A(\tau,\lambda)$ is approximated by the expression $[1 - T(\tau,\lambda)]/2.303$ for sufficiently low $T(\tau,\lambda)$ values. In general, transient absorbances arise from four different contributions,[31] excited-state absorption (ESA), stimulated emission (SE) and Raman gain (SRG) and bleaching (B). ESA is associated with the decrease of $I(\tau,\lambda)$ with respect to the incident intensity $I_0(\lambda)$ and then with positive transient absorbances, $\Delta A(\tau,\lambda) > 0$. Conversely, SE, SRG, and B correspond to the condition $I(\tau,\lambda) > I_0(\lambda)$ and therefore to $\Delta A(\tau,\lambda) < 0$.

The decay curves have been determined following two different sampling procedures. In the simplest, excited-state absorbances at a given wavelength are extracted from the limited number of transient absorption spectra actually measured. In the second a higher sensitivity is achieved (a) increasing the repetition rate and lowering the pump intensity and (b) making use of lock-in detection techniques. In this scheme, wavelengths are selected placing interference filters (fwhm ≈ 20 nm) along the probe beam beyond the solution cell and detecting the probe intensity with a silicon double-photodiode. A lock-in amplifier synchronized with a mechanical chopper operating at 500 Hz alternatively blocks the 1 kHz train of pump pulses and amplifies the probe signal when the excitation pulse is switched on. The relaxation dynamics is sampled with variable time steps starting from 50 fs in the first picosecond interval and ending to 1 ps in the interval 20−50 ps so that the sampling points for a given time interval are approximately constant. Increasing the delay, larger time steps were chosen between 500 and 1500 ps. Due to the high number of sampling points the second procedure was preferred to the first. The decay curves measured in the two cases have been found to be essentially coincident.

The relaxation kinetics has been studied on the basis of the following expression

$$\Delta A(\tau,\lambda) = \int_{-\infty}^{+\infty} g[(t-\tau),\lambda]\, R(t,\lambda)\, \mathrm{d}t \qquad (1)$$

where $\Delta A(\tau,\lambda)$ is the experimentally observed transient absorbance at the selected wavelength resulting from the convolution of the instrumental function $g[(t-\tau),\lambda]$ with the molecular response function $R(t,\lambda)$. The latter is further expanded in terms of exponential contributions as $R(t,\lambda) = \sum_i A_i(\lambda) \exp(-t/\tau_i)$, each component of which is characterized by the amplitude A_i and lifetime τ_i. The instrumental function is defined as cross-correlation between pump and probe pulses, $g(t) = \int I_{\mathrm{pump}}(t') I_{\mathrm{probe}}(t'+t)\, \mathrm{d}t'$, and determined measuring by stimulated gain the time profile of the solvent most intense Raman peaks. The CH mode of cyclohexane is observed at 2850 cm^{-1} and the ClO_4 symmetric stretching and OH modes of $HClO_4$ at ≈950 and 3520 cm^{-1}, respectively.[34] By plotting the intensity of the Raman signal vs the delay time, we show that the cross-correlation function has a Gaussian shape with temporal width (fwhm) 160 ± 10 fs. The temporal maximum of the cross-correlation function is a good indication of zero delay time at the absolute wavelength corresponding to the Raman line. At wavelengths different from those of the Raman lines, $g(t)$ has been determined by means of the time-resolved optical Kerr effect. Due to the reduced thickness of our cell it has been verified that the pulse width is independent of the probe wavelength. As a consequence, no correction has been applied to the previously measured instrumental function.

III. Results

First, we shortly review results[23] on the $S_0 \rightarrow S_n$ spectra of **1**−**3** that are pertinent to our study and supply additional information making reference to Figure 2. Under D_{4h} symmetry for **3** and D_{2d} symmetry for the lowest energy conformation[22,26,27] of **2** the two $\pi\pi^*$ states S_1 and S_2 are doubly degenerate, as they belong to E_u and E symmetry species, respectively. The $S_0 \rightarrow S_1$ and $S_0 \rightarrow S_2$ transitions are allowed and give origin to the Q and B bands. As to **3**, the maximum of the sharp B band has been reported[23] at 372.2 nm and the origin of the Q-band at 571.5 nm, so that the energy gap ΔE(B−Q) is ≈9370 cm^{-1}. The absorption spectrum of **2** depends on solvent because the B band shifts to 394.5 nm in benzene/cyclohexane solution from 401.8 nm in benzene.[23] No appreciable shift is seen for the Q-band and ΔE(B−Q) is estimated to be ≈8500 cm^{-1}. Lowering the molecular symmetry from D_{4h};D_{2d} to D_{2h} in **1** splits each of the two excited states into two components, $B_{3u} + B_{2u}$. Four bands are expected, Q_x (B_{3u});Q_y (B_{2u}) and B_x (B_{3u});B_y (B_{2u}), although experimentally the splitting is observed only for the Q_x;Q_y pair. The Soret maximum is found at 393.1 nm and the Q_x and Q_y origins at 617.7 and 517.0 nm, giving $\Delta E(B-Q_y) \approx 6100$ cm^{-1} and $\Delta E(B-Q_x) \approx 9250$ cm^{-1}.

1. Porphyrin. The transient absorption spectra of **1** ($c = 3 \times 10^{-5}$ M in benzene/cyclohexane 1:10; room temperature) exciting on the rising edge of the Soret band, 400 nm, have been measured as a function of the delay time between probe and pump pulse up to 1.5 ns. The time evolution of these spectra is shown in Figure 3, where spectral results before and after 5 ps are displayed separately. The spectrum shown with the solid line in the lower panel of Figure 3 is observed when pump and probe pulses are temporally coincident. As anticipated in the previous section, the negative signal at 451.5 nm, 2850 cm^{-1} from the 400 nm excitation pulse, is due to SRG of the CH stretching mode of solvent cyclohexane and overlaps the unstructured ESA signal. Other negative absorbances appear with increasing delay times (whereas the SRG peak disappears within 200 fs) and are easily assigned as bleachings of the Q_x and Q_y bands. In the upper inset of Figure 3 the transient spectrum at the delay time of 1.5 ns displays also the negative Q_x origin peak at 616 nm to which both B and SE contribute.

Two ESA bands are observed with maxima at 412 and 465 nm, whose the first is severely distorted due to the onset of the Soret absorption so that no band maximum survives above 400 nm once account is taken of the Soret bleaching. The two signals show strongly different kinetic behaviors, as reported in separate panels of Figure 4. The transient at 465 nm rises within the time resolution of our apparatus and decays in ≈600 fs to a nonvanishing background level. By applying the deconvolution/fitting procedure, we were unable to resolve the ultrafast formation of the state responsible for this signal. The decay time of the 465 nm ESA band has been confidently fitted to 150 ± 40 fs. As to the relaxation dynamics of the transient at 412 nm, four different components contribute to the signal. The biexponential growth with time constants 140 ± 40 fs and 1.8 ± 0.3 ps is followed by two decay processes in different time scales, the first with a lifetime of 25 ± 3 ps and a second too long to be measured accurately with our apparatus but consistent with the lifetime of the Q_x state, 10.7 ns in a nondegassed benzene solution.[23]

Finally, exciting into the Q_y vibronic band at 490 nm, transient spectra in the range 410−480 nm have been obtained. Due to the low absorbance of the Q_y band and difficulties to separate spatially the pump from the probe beam, the transient spectra of Figure 5 have a spectral quality lower than those of Figure 3. Nevertheless, the spectra obtained at early delay times indicate conclusively that the two ESA bands at 412 and 465 nm are due to starting states different from B.

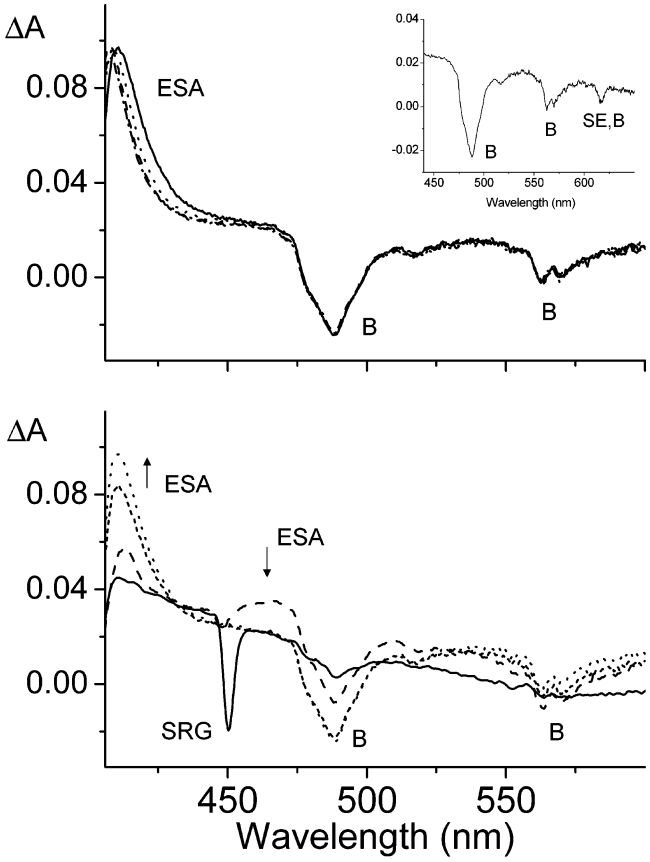

Figure 3. Transient absorption spectra of **1** ($c = 3 \times 10^{-5}$ M in benzene/cyclohexane 1:10, room temperature) in the spectral range 400−600 nm exciting at 400 nm with femtosecond pulses. The transient spectra are plotted as a function of the delay time between pump and probe pulses. The ESA, SRG, B, and SE symbols identify transient bands due to excited-state absorption, stimulated Raman gain of the solvent, bleaching, and stimulated emission, respectively. (Lower panel) transient spectra in the first 5 ps: solid line, temporal coincidence between pump and probe pulses; long dashed, short dashed, dotted lines, 200 fs, 1 ps, 5 ps delay times, respectively; vertical arrows up and down, intensity increase and decrease with time. (Upper panel) transient spectra after 5 ps delay time: solid, dotted, short dashed, dash-dotted lines, 5, 20, 100, 500 ps delay times, respectively. Inset of the upper panel: transient absorption spectrum at 1.5 ns delay time.

2. Diprotonated Porphyrin. The transient absorption spectra of **2** ($c = 2 \times 10^{-5}$ M in benzene/cyclohexane 1:10; 5% trifluoroacetic acid; room temperature) in the same experimental conditions as for **1** are collected in Figure 6. The transient spectrum exhibits a well shaped ESA band around 440 nm and a long unstructured tail extending up to 525 nm. The bleaching of the Q-band is observed at 543 nm. The transient intensity slowly decreases in the picosecond time scale, but the spectral shape is unaffected.

The relaxation dynamics has been characterized by measuring the kinetic profiles at 440 and 500 nm. The results are shown in Figure 7. Three dynamic processes contribute to the time evolution of these signals in distinct temporal domains: the formation of a transient in hundreds of femtoseconds, a second process in the picosecond range and a decay of several nanoseconds. The time constants have been calculated by means of our deconvolution/fitting program as $\tau_1 = 300 \pm 50$ fs, $\tau_2 = 9 \pm 2$ ps, and $\tau_3 = 5.5$ ns. The latter value has been kept

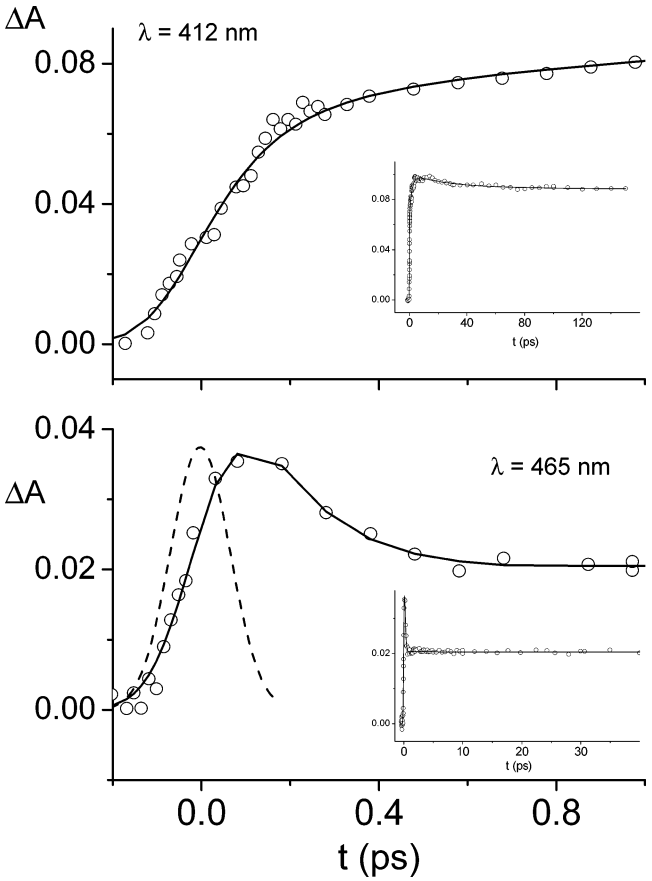

Figure 4. Transient absorbance of **1** as a function of the delay time in the same experimental conditions detailed in Figure 3 and probing at 465 nm (lower) and 412 nm (upper). In the lower panel the cross-correlation Gaussian profile (fwhm = 160 fs) between pump and probe pulses is also reported as dashed line. The insets of the two panels show the transient absorbances at the probe wavelengths 412 and 465 nm for long delay times.

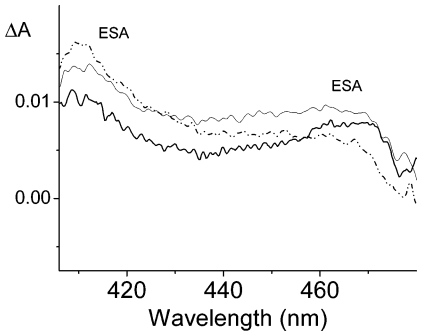

Figure 5. Transient absorption spectra of **1** in the same experimental conditions detailed in Figure 3 in the spectral range 410−480 nm exciting at 490 nm with femtosecond pulses. The transient spectra are plotted as a function of the delay time between pump and probe pulses. The ESA symbol identifies transient bands due to excited-state absorption. Key: solid thick line, temporal coincidence between pump and probe pulses; solid thin and dashed-doubly dotted lines, 100 and 400 fs delay times.

constant in the fitting procedure and equal to the already reported Q lifetime in the nondegassed solution.[29,23] The shortest time τ_1 corresponds for both kinetic profiles to a rise time, and the second time τ_2 has positive amplitude at 500 nm and negative amplitude at 440 nm. This means that τ_2 is the decay time at 500 nm and the rise time at 440 nm of the same relaxation process.

3. Tetraoxaporphyrin Dication. The transient absorption spectra of **3** ($c = 6 \times 10^{-6}$ M in concentrated $HClO_4$; room temperature) exciting at 370 nm, i.e., on the maximum of the Soret band, shows a remarkably well structured ESA doublet at 405 and 425 nm for delay times ≥20 ps, as it can be seen from Figure 8. The intensities of the two components increase simultaneously and reach the maximum at about 100 ps. Beyond this time the intensity of the transient spectrum lowers; however, the profile remains unaltered (see the inset of Figure 8). At zero delay time the negative 429 nm peak, assigned as SRG of the 3520 cm^{-1} OH stretching vibration of $HClO_4$, is observed. A second negative band around 525 nm is assigned as bleaching of the vibronic Q-band. The kinetic profiles of the 405 and 425 nm ESA signals, reported in Figure 9, are reproduced by the convolution of the exciting pulse with a single rise process with time constant 25 ± 5 ps and a single decay process with time constant 7.2 ns. The latter value is coincident with the fluorescence lifetime of the Q state.[23]

Blue shifts of the band maxima have been observed as a function of the delay time for the intense ESA bands of **2** and **3** at 440 and 425 nm, respectively. For simplicity the results are collectively reported in Figure 10. The plots, although not determined with high accuracy due to the scarcity of data points, are reasonably fit to single exponentials with time constants in

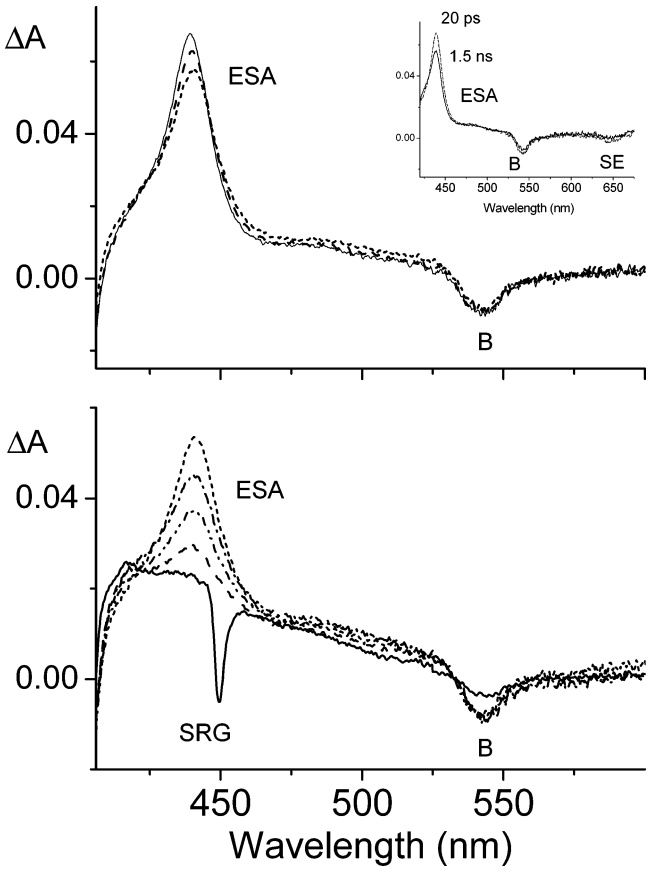

Figure 6. Transient absorption spectra of **2** ($c = 2 \times 10^{-5}$ M in benzene/cyclohexane 1:10, 5% trifluoroacetic acid, room temperature) in the spectral range 400−600 nm exciting at 400 nm with femtosecond pulses. The transient spectra are plotted as a function of the delay time between pump and probe pulses. The ESA, SRG, B, and SE symbols identify transient bands due to excited-state absorption, stimulated Raman gain of the solvent, bleaching, and stimulated emission, respectively. (Lower panel) transient spectra in the first picosecond: solid line, temporal coincidence between pump and probe pulses; long dashed, dashed-doubly dotted, dashed-dotted, short dashed lines, 200, 400, 600 fs, 1 ps delay times, respectively. (Upper panel) transient spectra after 1 ps delay time: short dashed, long dashed, solid lines, 2, 10, 20 ps delay times. Inset of the upper panel: transient absorption spectra at 20 ps and 1.5 ns delay times.

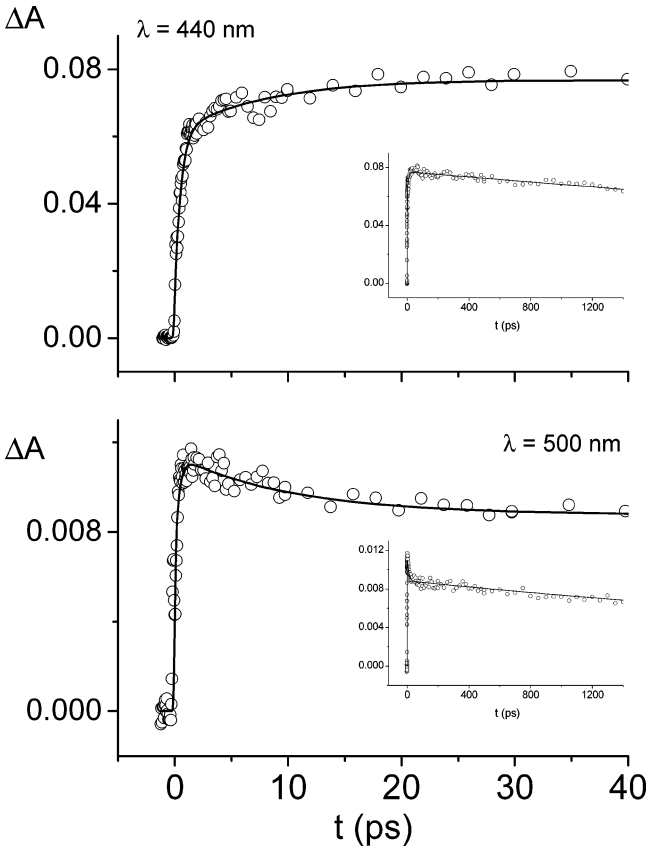

Figure 7. Transient absorbance of **2** as a function of the delay time in the same experimental conditions detailed in Figure 6 and probing at 500 nm (lower) and 440 nm (upper). The insets of the two panels show the transient absorbances at the probe wavelengths 500 and 440 nm for long delay times.

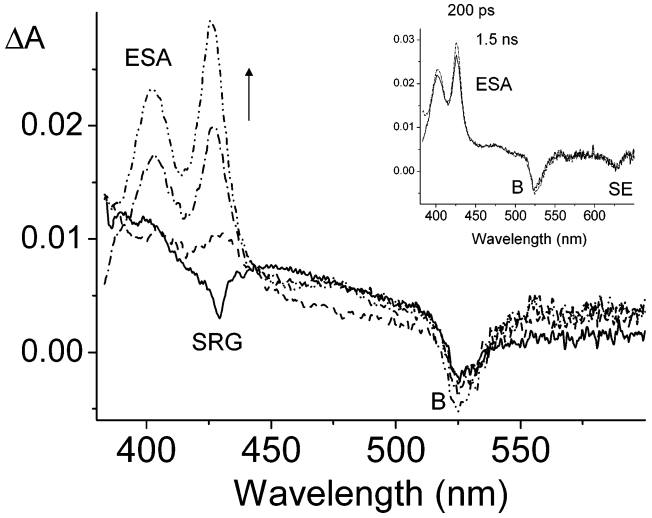

Figure 8. Transient absorption spectra of **3** ($c = 6 \times 10^{-6}$ M in concentrated $HClO_4$, room temperature) in the spectral range 400−600 nm exciting at 370 nm with femtosecond pulses. The transient spectra are plotted as a function of the delay time between pump and probe pulses. The ESA, SRG, B, and SE symbols identify transient bands due to excited-state absorption, stimulated Raman gain of the solvent, bleaching, and stimulated emission, respectively. Key: solid line, temporal coincidence between pump and probe pulses; long dashed, dashed-dotted, dashed-doubly dotted, 5, 20, and 200 ps delay times, respectively; vertical arrow up, intensity increase with time. Inset: transient absorption spectra at 200 ps and 1.5 ns delay times.

the range 10−30 ps, i.e., ≈22 ps for **2** and ≈11 ps for **3**. Similar band shifts have been reported for vibrationally excited porphyrins and interpreted as due to thermalization of the "hot" distribution of vibrational states by internal relaxation and energy dissipation to the solvent environment.[35−37]

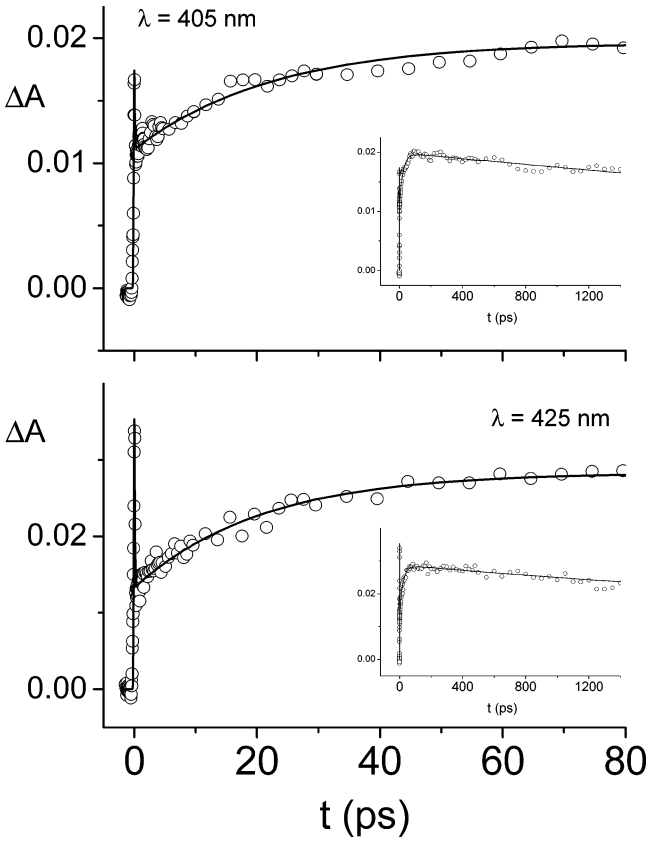

Figure 9. Transient absorbance of **3** as a function of the delay time in the same experimental conditions detailed in Figure 8 and probing at 425 nm (lower) and 405 nm (upper). The insets of the two panels show the transient absorbances at the probe wavelengths 425 and 405 nm for long delay times. A two-photon spike is observed for both transient absorbances when the pump and probe pulses temporally overlap.[46,47]

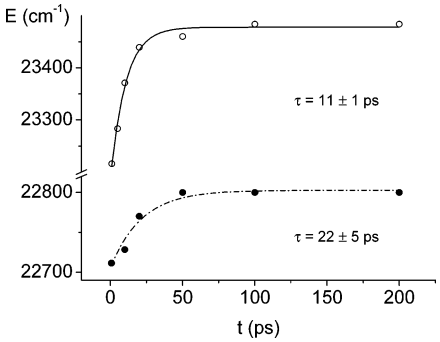

Figure 10. Dynamic blue shifts [E (cm^{-1})] of the ESA bands at 440 nm, for **2**, and at 425 nm, for **3**, as a function of the delay time. The data for **2** and **3** are reported as full and hollow circles, respectively. The time constants (τ, ps) of thermal equilibration in the Q state are indicated.

IV. Discussion

Considering first porphyrin **1** the analysis of our data follows closely previous studies.[10,12] We have found that **1** decays from the Soret band within the time resolution of our apparatus, 160 fs, therefore leading to the conclusion that the time constant of the B → Q_y internal conversion occurs in the tens of femtoseconds time regime. In fact, no rise component is resolved for the 465 nm ESA signal. In porphyrin derivatives an upper limit

TABLE 1: Multiexponential Fittings of the Observed Kinetic Profiles Shown in Figures 4, 7, and 9: Time Constants (τ, ps), Amplitudes (A), and Wavelengths (λ_{probe}, nm)[a]

1			2			3		
λ_{probe}	A	τ	λ_{probe}	A	τ	λ_{probe}	A	τ
412	−0.06 −0.03 0.01 0.09	0.14 ± 0.04 1.8 ± 0.3 25 ± 3 10.7[b]	440	−0.05 −0.016 0.08	0.30 ± 0.05 9 ± 1 5.5[b]	405	−0.009 −0.02	25 ± 3 7.2[b]
465	0.037 0.02	0.15 ± 0.04 10.7[b]	500	−0.05 0.026 0.009	0.33 ± 0.05 9 ± 1 5.5[b]	425	−0.015 0.029	25 ± 3 7.2[b]

[a] Decay processes correspond to positive amplitudes and rise processes to negative amplitudes. [b] Time constants in nanoseconds held fixed in the multiexponential fitting.

of ≈40−50 fs has been estimated for the B → Q_y internal conversion.[10,12] Going further, the decay time of the 465 nm transient is coincident, within the experimental accuracy, with the shortest rise time of the 412 nm transient. This means that the Q_y depopulation is coupled with a population growth relative to the manifold of Q_x vibrational levels quasi-degenerate with Q_y. Accordingly, the two kinetic behaviors correspond to the same deactivation channel, i.e., Q_y → Q_x internal conversion with time constant of ≈150 fs. This time is unresolvably short in H_2TPP[10] and stretches to 90 fs in the more complex derivative having two phenyl substituents on opposite *meso* positions and methyl or ethyl groups in all β positions.[12] Thus, the internal conversion rate increases from **1** to H_2TPP, roughly depending upon the number of phenyl substituents along the ring periphery. Also the subsequent decay processes are slower in **1** than in the derivatives. Time constants of 1.4 and 1.5 ps have been measured for the two substituted porphyrins and attributed to vibrational energy relaxation in the Q_x state.[10,12] In the case of **1** the time constant results to be slightly longer, 1.8 ps. The substituent effect is even larger for the last process occurring in Q_x before fluorescence, i.e., thermal equilibration with the solvent. The time constant of 25 ps for **1** exceeds appreciably the reported value for H_2TPP, which is in the range 10−20 ps.[10]

Going from **1** to **3** the molecular symmetry increases from D_{2h} to D_{4h} so that, as already pointed out in the Results section, the Q and B states are doubly degenerate, of E_u symmetry species, and with an energy separation much larger than between B and Q_y. A single rise process of 25 ps time constant is observed before fluorescence, indicating that the population of the thermally equilibrated Q state increases in the picosecond time scale. As to the B lifetime, an upper limit of ≈100 ps has been reported.[23] This parameter has been also estimated[23] from quantum yield measurements on highly diluted (≈10^{-7} M) solutions to be ≈40 ps. Considering that the indirect determination has uncertainty width larger than the direct time-resolved measurement, it is reasonably concluded that the rise of the Q fluorescence is correlated with the decay of the B fluorescence. Vibrational relaxation, which is known to take place in few picoseconds or less in the excited states,[38] is too fast to be resolved with respect to internal conversion. Also, the thermal equilibration component may be deconvoluted from the total rise process, assuming a time constant as indicated by the dynamic band shift, without altering substantially the time constant of the internal conversion. The dramatic increase of this constant from ≈50 fs in **1** to ≈25 ps in **3** is related to the increase of the energy gap ΔE(B−Q).[39] In other words, no additional singlet states between B and Q contribute to the decay. In this respect, we note that the energy level diagram of **3** is similar to that of D_{4h} metalloporphyrins, the only difference being the reduced gap in the latter systems. This leads to speculate about a possible correlation between the internal conversion rate constants of **3** and of metalloporphyrins. B fluorescence lifetimes have been reported[16,40] for Zn(II) and Mg(II) TPP in various solvents for which ΔE(B−Q) ranges between 6300 and 7100 cm^{-1}. The rate constants, calculated at moderate/small fluorescence quantum yields as reciprocal lifetimes,[16] have been plotted in Figure 11 in a semilogaritmic scale vs ΔE(B−Q) with addition of the equivalent rate for **3**. As the latter value falls close to the semilogaritmic linear plot, it is tempting to propose that the 25 ps lifetime fairly corresponds to that of the D_{4h} porphyrin macrocycle isoelectronic with **3** in absence of the central metal atom.

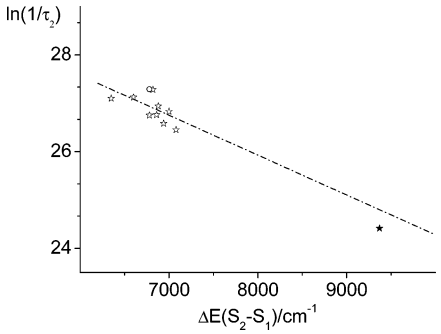

Figure 11. Internal conversion B → Q rate constant $1/\tau_2$ vs energy gap between the two states [$\Delta E(S_2-S_1)$, cm^{-1}] in a semilogaritmic scale. Stars and hollow circle refer to data for Zn(II) and Mg(II) tetraphenylporphyrins in various solvents; data taken from refs 16 and 40. The full star is the value of the rate constant for **3** determined in this work. The dashed-dotted plot has been obtained from the linear regression of data on metalloporphyrins.

Diprotonated porphyrin **2** is a case more complex than **1** and **3**. In fact, because the rate of the internal conversion depends on the separation energy between the two states[39] and this value, 8500 cm^{-1} for **2**, is comparable, though smaller, to that of **3** while much greater than that of **1**, we would be inclined to associate the observed time constant of 9 ps with the B → Q decay. On the other hand, the B lifetime has been estimated to be ≈150 fs from fluorescence yield and radiative lifetime.[23,29] In our opinion, the difference between 150 fs and 9 ps is too large to be attributed to inaccuracies of the indirect estimate, as proposed for **3**. Instead, decay processes more efficient than the B → Q internal conversion are operative in the present case. In fact, it should be recalled that nonplanar porphyrins, such as dodecaphenyl- and tetra-*t*-butylporphyrin have strongly reduced Q lifetimes with respect to those of substituted planar porphyrins.[24,28] The effect was attributed to the torsional flexibility of **2** in the Q state.[24,28] The conformational freedom causes the shift to excited-state configurations for which the vertical energy gap with the ground state is smaller than that at the equilibrium Q geometry, thus enhancing the rate of internal conversion.[41] A similar mechanism may be invoked for the B state. As a second point, it has been shown[23] that not only B but also

charge-transfer (CT) states are responsible for the fluorescence emission of **2** in the region 420−550 nm. The latter are described as states of the complex $H_4P^{2+}(CF_3COO^-)_2$ where one electron is promoted from occupied MOs localized on the trifluoroacetate counterion to virtual MOs localized on the porphyrin macrocycle.[23,26,42] Because CT states are interspersed between B and Q, the internal conversions B → CT and then CT → Q provide a more effective deactivation mechanism than the direct B → Q channel. Following these considerations, we attribute the ultrafast 300 fs decay to a combination of factors, B → CT conversion and, probably to a lesser extent, B → Q conversion through distorted B configurations. The second conversion CT → Q occurs with time constant 9 ps. We know that the thermally equilibrated Q state is reached within ≈22 ps. With complete analogy to the case of **3**, fitting the two kinetic profiles of Figure 7 with inclusion of thermal equilibration has little effect on the time constant of the CT → Q internal conversion. Summarizing, due to presence of intruder CT states, the decay mechanism in **2** is intrinsically different from that of **3**. In fact, the rate constant corresponding to the 300 fs lifetime is at strong variance with those reported in Figure 11. Thus, we conclude that although the lowest energy conformation of diprotonated porphyrin has fourfold (improper) symmetry[22,26,27] and low-lying $\pi\pi^*$ states of double degeneracy, inference about similarity of decay mechanisms in the two cases is misleading.

V. Conclusions

In this paper we have reported on the relaxation dynamics of porphyrin **1**, diprotonated porphyrin **2**, and tetraoxaporphyrin dication **3** following the ultrafast excitation of these molecules in solution into the Soret band at room temperature. A series of distinct decay processes including thermal equilibration in the lowest excited state have been resolved. Internal conversion from the B (or Soret) state to the adjacent lower state plays the most remarkable role. As the energy separation widens from $\Delta E(B-Q_y) \approx 6100\ cm^{-1}$ in **1** to $\Delta E(B-Q) \approx 9370\ cm^{-1}$ in **3**, the time constant of the internal conversion increases from ≤50 fs to 25 ps, with a variation of more than 2 orders of magnitude. On the other hand, internal conversion in **2** involves charge-transfer (CT) states lying energetically between B and Q. These states favor the B → Q decay through the indirect step B → CT, thus bypassing the constraint imposed by the energy gap $\Delta E(B-Q)$, comparable to that of **3**. As a consequence, the time constant for the B → Q decay of **2** goes back to 300 fs. The correlation of B lifetimes of **3** and of some metalloporphyrins in various solvents suggests that the B → Q internal conversion in **3**, occurring in the picosecond time scale, is representative of the process in the hypothetical bare macrocycle of metalloporphyrins.

As a final comment, we emphasize the fact that the experimental results reported in this paper offer the possibility to discuss a second important point on **1**−**3**, i.e., the assignment of higher excited electronic states that are not usually reached in experiments performed with standard UV−vis absorption instrumentation. Few studies have been published on the issue and mostly addressing excited-state absorption of metalloporphyrins and porphyrins analogues/aggregates.[13,17,43−45] The assignment of the transient spectra included in this paper is currently under way in our group.

Acknowledgment. We are grateful to Prof. E. Vogel (University of Köln, Germany) for the generous gift of a sample of tetraoxaporphyrin perchlorate. This work was supported by INSTM under the contract FIRB RBNE033KMA and by the European Community under the contract RIII-CT-2003-506350.

References and Notes

(1) *The Porphyrins*; Dolphin, D., Ed.; Academic Press: New York, 1978; Vols. I−VII.
(2) *The Porphyrin Handbook*; K. Kadish, K., Smith, K., Guilard, R., Eds.; Academic Press: New York, 2002; Vol. 13.
(3) Gust, D.; Moore, T. A. In *The Porphyrin Handbook*; Kadish, K. M., Smith, K. M., Guilard, R., Eds.; Academic Press: Burlington, MA, 2000; Vol. 8, pp 153−190.
(4) Kuciauskas, D.; Liddel, P. A.; Lin, S.; Stone, S. G.; Moore, A. L.; Moore, T. A.; Gust, D. *J. Phys. Chem. B* **2000**, *104*, 4307−4321.
(5) D'Souza, F.; Gadde, S.; Islam, D.-M. S.; Wijesinghe, C. A.; Schumacher, A. L.; Zandler, M. E.; Araki, Y.; Ito, O. *J. Phys. Chem. A* **2007**, *111*, 8552−8560.
(6) Ogawa, K.; Zhang, T.; Yoshihara, K.; Kobuke, Y. *J. Am. Chem. Soc.* **2002**, *124*, 22−23.
(7) Thorne, J. R. G.; Kuebler, S. M.; Denning, R. G.; Blake, I. M.; Taylor, P. N.; Anderson, H. L. *Chem. Phys.* **1999**, *248*, 181−193.
(8) Kuebler, S. M.; Denning, R. G.; Anderson, H. L. *J. Am. Chem. Soc.* **2000**, *122*, 339−347.
(9) Sternberg, E. D.; Dolphin, D.; Bruckner, C. *Tetrahedron* **1998**, *54*, 4151−4202.
(10) Baskin, J. S.; Yu, H.-Z.; Zewail, A. H. *J. Phys. Chem. A* **2002**, *106*, 9837−9844.
(11) Zhong, Q.; Wang, Z.; Liu, Y.; Zhu, Q.; Kong, F. *J. Chem. Phys.* **1996**, *105*, 5377−5379.
(12) Akimoto, S.; Yamazaki, T.; Yamazaki, I.; Osuka, A. *Chem. Phys. Lett.* **1999**, *309*, 177−182.
(13) Aleman, E. A.; Rajesh, C. S.; Ziegler, C. J.; Modarelli, D. A. *J. Phys. Chem. A* **2006**, *110*, 8605−8612.
(14) Yu, H.-Z.; Baskin, J. S.; Zewail, A. H. *J. Phys. Chem. A* **2002**, *106*, 9845−9854.
(15) Gurzadyan, G. G.; Tran-Thi, T.-H.; Gustavsson, T. *J. Chem. Phys.* **1998**, *108*, 385−388.
(16) Gurzadyan, G. G.; Tran-Thi, T.-H.; Gustavsson, T. In *New Trends in Atomic and Molecular Spectroscopy*; Gurzadyan, G. G., Karmenyan, A. V., Eds.; SPIE vol. 4060; SPIE: Bellingham, WA, 2000; pp 96−103.
(17) Chosrowjan, H.; Taniguchi, S.; Okada, T.; Takagi, S.; Arai, T.; Tokumaru, K. *Chem. Phys. Lett.* **1995**, *242*, 644−649.
(18) Dietzek, B.; Maksimenka, R.; Kiefer, W.; Hermann, G.; Popp, J.; Schmitt, M. *Chem. Phys. Lett.* **2005**, *415*, 94−99.
(19) Sorgues, S.; Poisson, L.; Raffael, K.; Krim, L.; Soep, B.; Shafizadeh, N. *J. Chem. Phys.* **2006**, *124*, 114302.
(20) Kumble, R.; Palese, S.; Lin, V. S.-Y.; Therien, M. J.; Hochstrasser, R. M. *J. Am. Chem. Soc.* **1998**, *120*, 11489−11498.
(21) Osuka, A.; Lin, B.; Maruyama, K. *J. Org. Chem.* **1993**, *58*, 3582−3585.
(22) Jelovica, I.; Moroni, L.; Gellini, C.; Salvi, P. R.; Orlic, N. *J. Phys. Chem. A* **2005**, *109*, 9935−9944.
(23) Marcelli, A.; Foggi, P.; Moroni, L.; Gellini, C.; Salvi, P. R.; Badovinac, I. J. *J. Phys. Chem. A* **2007**, *111*, 2276−2282.
(24) Gentemann, S.; Medforth, C. J.; Forsyth, T. P.; Nurco, D. J.; Smith, K. M.; Fajer, J.; Holten, D. *J. Am. Chem. Soc.* **1994**, *116*, 7363−7368.
(25) Cheng, B.; Munro, O. Q.; Marques, H. M.; Scheidt, W. R. *J. Am. Chem. Soc.* **1997**, *119*, 10732−10742.
(26) Avilov, I. V.; Panarin, A. Y.; Chirvony, V. S. *Chem. Phys. Lett.* **2004**, *389*, 352−358.
(27) Chen, D.-M.; Liu, X.; He, T.-J.; Liu, F.-C. *Chem. Phys.* **2003**, *289*, 397−407.
(28) Gentemann, S.; Nelson, N. Y.; Jaquinod, L.; Nurco, D. J.; Leung, S. H.; Medforth, C. J.; Smith, K. M.; Fajer, J.; Holten, D. *J. Phys. Chem. B* **1997**, *101*, 1247−1254.
(29) Ohno, O.; Kaizu, Y.; Kobayashi, H. *J. Chem. Phys.* **1985**, *82*, 1779−1787.
(30) Vogel, E.; Haas, W.; Knipp, B.; Lex, J.; Schmickler, H. *Angew. Chem., Int. Ed. Engl.* **1988**, *27*, 406−409.
(31) Neuwhal, F. V. R.; Bussotti, L.; Foggi, P. In *Research Advances in Photochemistry and Photobiology*; Global Research Network: Trivandrum, India, 2000; Vol. 1, pp 77−94.
(32) Danielius, R.; Piskarkas, A.; Trapani, P. D.; Andreoni, A.; Solcia, L.; Foggi, P. *Appl. Opt.* **1996**, *35*, 5336−5339.
(33) Diels, J.-C.; Rudolph, W. *Ultrashort Laser Pulse Phenomena*; Academic Press: New York, 1996.
(34) Ross, S. D. *Inorganic Infrared and Raman Spectra*; McGraw-Hill: London, 1972.
(35) Rodriguez, J.; Holten, D. *J. Chem. Phys.* **1989**, *91*, 3525−3531.
(36) Rodriguez, J.; Kirmaier, C.; Holten, D. *J. Chem. Phys.* **1991**, *94*, 6020−6029.

(37) Bilsel, O.; Milam, S. N.; Girolami, G. S.; Suslick, K. S.; Holten, D. *J. Phys. Chem.* **1993**, *97*, 7216−7221.
(38) Elsaesser, T.; Kaiser, W. *Annu. Rev. Phys. Chem.* **1991**, *42*, 83−107.
(39) Englman, R.; Jortner, J. *Mol. Phys.* **1970**, *18*, 145−160.
(40) Karolczak, J.; Kowalska, D.; Lukaszewicz, A.; Maciejewski, A.; Steer, R. *J. Phys. Chem. A* **2004**, *108*, 4570−4575.
(41) Chirvony, V. S.; van Hoek, A.; Galievski, V. A.; Sazanovich, I. V.; Schaafsma, T. J.; Holten, D. *J. Phys. Chem. B* **2000**, *104*, 9909−9917.
(42) Knyukshto, V. N.; Solovyov, K.; Egorova, G. D. *Biospectroscopy* **1998**, *4*, 121−133.
(43) Khairutdinov, R. F.; Serpone, N. *J. Phys. Chem. B* **1999**, *103*, 761−769.
(44) Tobita, S.; Kaizu, Y.; Kobayashi, H.; Tanaka, I. *J. Chem. Phys.* **1984**, *81*, 2962−2969.
(45) Rodriguez, J.; Kirmaier, C.; Holten, D. *J. Am. Chem. Soc.* **1989**, *111*, 6500−6506.
(46) Dobryakov, A.; Kovalenko, S.; Ernsting, N. *J. Chem. Phys.* **2005**, *123*, 044502.
(47) Lorenc, M.; Ziolek, M.; Naskrecki, R.; Karolczak, J.; Kubicki, J.; Maciejewski, M. *Appl. Phys. B* **2002**, *74*, 19−27.